BASE DRAG OF NONCIRCULAR IRREGULAR SHAPED BODIES AT HIGH SPEEDS

SERDAREVIC-KADIC S., SOFTIC A. & RAZIC F.

Abstract: *If flow velocity equals sound velocity, base drag coefficient is a significant part of drag coefficient and it depends on variety of flow and geometrical parameters. Drag, base drag, drag coefficient and base drag coefficient for four bodies with same width, height and length and different shape are estimated by CFD (ANSYS Fluent) at high speeds. For different rear surface curvature, at high flow velocity, share of base drag at drag of body and flow field as contour of vector of velocity coloured by pressure are shown and analysed.*

Key words: *Irregular shaped body, Mach number, Base drag coefficient, Underpressure, CFD*

Authors´ data: Assistant Prof. Dr. Sc. Serdarevic-Kadic S[abina], Associate Prof. Dr. Sc. Softic A[lmira] & Razic F[aruk], Faculty of Mechanical Engineering, University of Sarajevo, Vilsonovo setaliste 9, Sarajevo 71000, Bosnia and Herzegovina, serdarevic@mef.unsa.ba, softic@mef.unsa.ba, razic@mef.unsa.ba.

This Publication has to be referred as: Serdarevic-Kadic, S[abina]; Softic, A[lmira] & Razic, F[aruk] (2022). Base Drag of Noncircular Irregular Shaped Bodies at High Speeds, Chapter 06 in DAAAM International Scientific Book 2022, pp.075-084, B. Katalinic (Ed.), Published by DAAAM International, ISBN 978-3-902734-34-1, ISSN 1726-9687, Vienna, Austria
DOI: 10.2507/daaam.scibook.2022.06

1. Introduction

Aerodynamic drag on a body moving through an air is generated by pressure and shear stress distributions on the body surface. Pressure acts normal to surface and shear stress acts tangential to the surface. According to basic sources of drag formation, the drag of body can be divided to the following components: the pressure drag and the viscous drag on the wet surface of body, and drag due to underpressure on the dry surface of body.

Base drag is influenced by a variety of flow and geometrical parameters. With turbulent boundary layer ahead of the base the major factors include: Mach number in the free stream, just ahead of the base; boundary layer momentum thickness ahead of the base; base diameter; angle of attack; afterbody shape (boat-tail or flare angle, forebody diameter, afterbody length); and parameters characterising the base drag reduction device (Suliman, et al., 2009).

Base drag arise from pressure on the afterbody or base caused by the separation of the flow from the body surface. Depending on the geometry, this separation creates either an annular or planar mixing-layer which is bounded on one side by a recirculation region. Due to discontinuity of surface, an expansion wave develops from the edge of base. The mixing layer converges towards a stagnation point in a high pressure region where the wake starts. The change in the direction of the streamlines in the vicinity of the stagnation point creates recompression waves. The complex dynamic interactions are inherently unsteady with high turbulent energy levels, as well as associated absolute and convective instabilities (Gatski & Bonnet, 2013).

Some of the difficulties in the prediction of base drag have included: (1) the upstream effects of the presence of a corner in various Mach number flows at different Reynolds numbers, (2) the effects of separation, compression and/or expansion, and shock formation in the vicinity of the corner, (3) the structure of the recirculating zone, (4) the formation and structure of a mixing (shear) layer between the recirculating zone and the external flow, and (5) the effects of the configuration. Detailed experimental investigations of the unsteady flow field of transonic and supersonic base flows are technically challenging and expensive (Serdarevic-Kadic & Terzic, 2019).

Measurements in separated flows are generally difficult and most experimental studies in the literature have provided only information about the base pressure (or drag) and certain mean properties of the near-wake-like velocity profiles or static pressure variations on the wake centreline (Sivasubramanian & Fasel, 2006). The desire to increase weapon range and manoeuvrability, design weapons that are more optimum from an aircraft total drag and radar signature standpoint, or provide optimum loadout of multiple missiles in a ship's vertical launcher has driven weapons designers to consider nonaxisymmetric body shapes. Current state-of-the-art methods for predicting aerodynamics of nonaxisymmetric body shapes with engineering accuracy are much more limited than for axisymmetric bodies (Moore, 2000).

A method for prediction aerodynamics of elliptic cross-sectional shapes to any angle of attack and other cross-sectional shapes at small angle of attack (Jorgensen, 1973) was derived on the basis of slender body theory for low angle of attack and modified Newtonian theory at higher angle of attack.

Jorgensen assumes that axial force coefficient at zero angle of attack of the equivalent axisymmetric body is same as that for the noncircular body and that axial force coefficient varies with square cosine of angle of attack. These assumptions need further investigation (Moore, 2000).

Twisdale and Vickery (Twisdale & Vickery, 1992) applied modified cross-flow theory to develop the expression for drag coefficient of the random orientation rectangular parallelepiped as function of orientation angles and geometrical characteristics.

Moxnes et al. (Moxnes, 2017) showed different novel analytical models for expected projected area and drag coefficient of irregular shaped bodies like fragments that tumble or rotate with the rotational axis normal to the velocity vector. They forecasted a model where the expected drag coefficient depends on shape and Mach number.

Murman (Murman, 2010) presented a method for predicting the drag of unconstrained bluff bodies from subsonic through supersonic flight conditions using analytic expressions.

McCleskey (McCleskey, 1988) calculated drag coefficient from individual test records for 96 irregular shaped bodies (fragments) tested in the vertical wind tunnel at low subsonic speed.

However, there are no available data on the drag coefficient and its components for non-slender irregular shaped bodies at high speeds. The ability to compute the base region flow field for different configurations using Navier-Stokes computational techniques has been developed over the past few decades, so the Computational Fluid Dynamics (CFD) becomes an attractive alternative to expensive experiments.

The primary purpose of the paper is to determine base drag coefficient of non-slender noncircular irregular shaped bodies at high speeds, its share to the total drag coefficient and its behaviour depending on the Mach number. The secondary objective is to determine how much the curvature of base affects to base drag coefficient for noncircular irregular shaped bodies at different speed regimes.

2. Computational Method

The drag force is defined in terms of this drag coefficient as:

$$D = \frac{1}{2}\rho \cdot V^2 \cdot A_{ref} \cdot C_D \tag{1}$$

where: ρ is freestream density, V is freestream velocity, A_{ref} is reference area and C_D is aerodynamic drag coefficient. Reference area is chosen to pertain to the given geometric body shape. If it is assumed that outer surface of the body in air flow consists of wet surface S_w (surface in contact with air) and dry surface S_d, then the drag coefficient can be written as:

$$C_D = C_{D_w} + C_{D_{sf}} + C_{D_b} \tag{2}$$

where: C_{D_w} is pressure drag coefficient due to wet surface, $C_{D_{sf}}$ is skin friction drag due to wet surface and C_{D_b} is pressure drag coefficient due to dry surface.

In this study, 4 irregular shaped bodies with noncircular cross section are taken under consideration: three-axis ellipsoid (ellipsoid), short cylinder with elliptic-shaped base (short elliptic cylinder), long cylinder with elliptic-shaped base (long elliptic cylinder) and parallelepiped. These bodies have same dimensions: width $a = 68$ mm, height $b = 17.3$ mm and length $c = 12$ mm and they are shown at Fig. 1. Ellipsoid and short elliptic cylinder have reference area $A_{ref} = (ab/4) \cdot \pi$, and parallelepiped and long elliptic cylinder have reference area $A_{ref} = ab$. Body dimensions are chosen because drag force values of three-axis ellipsoid with the same dimensions are available. Choice of body shape is made with purpose of noticing the influence of flat surface, curved surface and sharp edge on base drag coefficient.

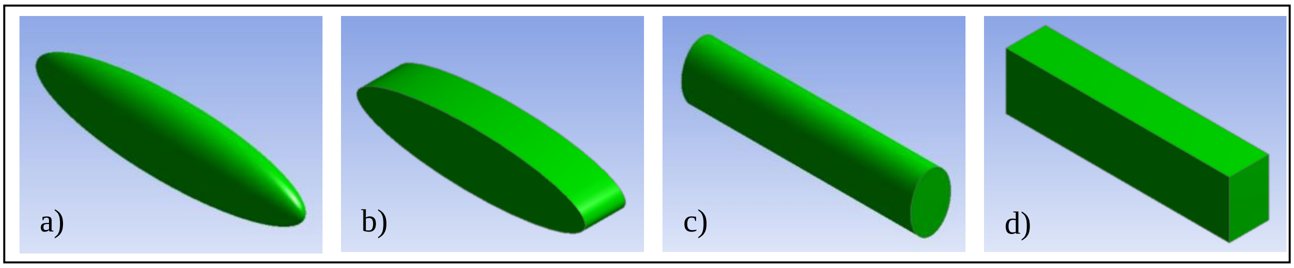

Fig. 1. Irregular shaped bodies with noncircular cross area: a) three-axis ellipsoid; b) short elliptic cylinder; c) long elliptic cylinder; d) parallelepiped.

Numerical simulation of flow field around bodies is obtained with the computational fluid dynamics software ANSYS Fluent. The following is adopted for all simulations:

- The working fluid is air, an ideal gas, which is modified in accordance with compressibility and changes of thermosphysical characteristics with temperature. Density and viscosity depend on temperature, and c_p and thermal conductivity are considered as constants.
- Pressure and temperature of air free flow correspond to parameters of air at sea level according to the standard atmosphere ICAO, $p = 101325\ Pa$ and $T = 288\ K$.
- Direction of airflow is assumed to be perpendicular to maximum cross section of the body (reference area).
- Flow around the body is compressible and turbulent.

Numerical method that simultaneously solves the equation of continuity, equation of momentum and energy equation is used. This method is developed for high velocity compressible flows. The governing equations are linearized by implicit manner. For a given variable, the unknown value in each cell is computed using a relation that includes both existing and unknown values from neighbouring cells. Therefore, each unknown variable will appear in more than one equation in the system, and these equations must be solved simultaneously to give the unknown quantities.

Spalart- Allmaras model is selected for turbulence modelling. Solution of Navier-Stokes equations was done by using 3-dimensional density based solver.

Spatial domain is divided into two parts, inner and outer. Discretization of spatial domain inner part is performed by non-uniform unstructured mesh and discretization of spatial domain outer part is performed by non-uniform structured mesh, as shown at Fig. 2.

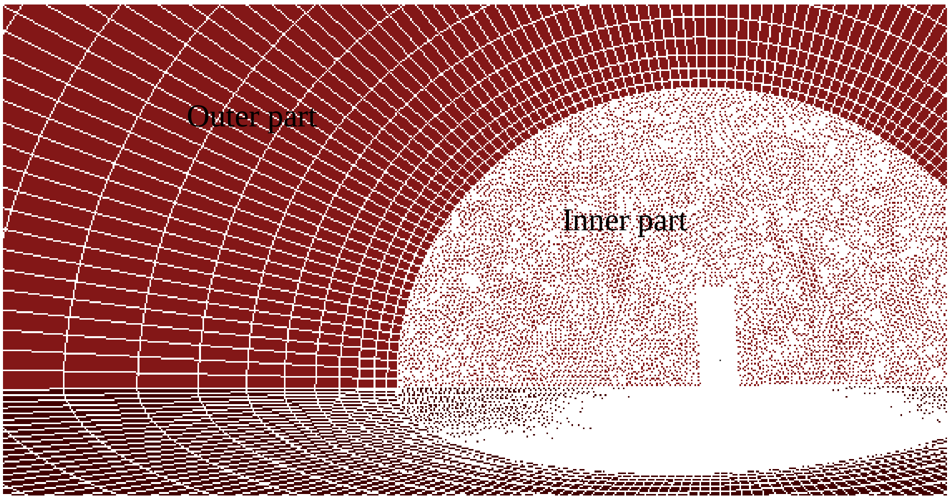

Fig. 2. Discretization of spatial domain

Chosen bodies have three planes of symmetry and expected flow images are symmetrical to two planes, so the simulations were made on one quarter of the body with the purpose of decreasing number of mesh cells and time of calculation.

Computational domain is limited to the body contour, two symmetry planes and outer boundary. Radius of outer boundary is more than 10 times body maximum dimension.

Following types of boundary are chosen:

- „Wall" boundary, which is used to delimit the regions of fluid and solid, is set to body contour.
- „Symmetry" boundaries are used as symmetry planes.
- „Pressure far field" boundary, which is used for modelling of compressible free flow parameters at the infinity, is set on the outer boundary of computation domain.

Wall boundary of ellipsoid and wall boundary of long elliptic cylinder are divided into 2 parts: front surface and rear surface by maximum cross section during geometry modelling. Exterior surfaces of short elliptic cylinder and parallelepiped are divided into 3 parts: front surface, middle section surface and rear surface.

The verification of the model was made on the basis of three-axis ellipsoid drag force (Kljuno & Catovic, 2019). Deviation of results is not greater than 3.5%. The most important reasons for the deviation of results are different free flow temperature, different mesh and different radius of outer boundary.

Twenty simulations were made, five for each body. Simulations were made for $M = 1; 1.2; 1.5; 1.8$ and 2.

3. Results and discussion

Drag force coefficient has three components which are generated by pressure of the air as it is compressed on the body surface, friction of the air as it passes over the body and the pressure on the afterbody or base by the separation of the flow from the body surface. All of the individual drag force components are computed simultaneously as part of the solution.

According to geometry of body and division into front, middle section and rear surface, for each part of body, drag force due to pressure and drag force due to shear stress are estimated and shown in Fluent force report for direction vector of flow velocity. Drag force is a sum of drag forces due to pressure and shear stress for all parts of a body. Drag force at rear surface due to pressure is in fact base drag force.

Drag force coefficient and base drag coefficient are calculated by the definition of aerodynamic force coefficient which follows from equation (2) and for value of reference area which is entered as reference value during the problem setup in Fluent.

The simulation results are grouped according to the maximum cross section area of the bodies. Values of drag force D, base drag force D_b, aerodynamic drag coefficient C_D and aerodynamic base drag coefficient C_{D_b} as function of Mach number for ellipsoid and short elliptic cylinder are shown at table 1 and these values for parallelepiped and long elliptic cylinder are shown at table 2.

Mach No.	Ellipsoid				Short elliptic cylinder			
	D $[N]$	D_b $[N]$	C_D	C_{D_b}	D $[N]$	D_b $[N]$	C_D	C_{D_b}
1	94.57	47.85	1.444	0.731	114.61	39.97	1.750	0.610
1.2	141.23	57.41	1.498	0.609	168.89	49.06	1.791	0.520
1.5	219.72	65.87	1.491	0.447	265.76	57.96	1.804	0.393
1.8	310.86	70.75	1.465	0.333	380.34	63.83	1.793	0.301
2	378.63	72.43	1.445	0.276	458.91	66.45	1.752	0.254

Tab. 1. Drag and drag coefficient as function of Mach number for ellipsoid and short elliptic cylinder by CFD.

Mach No.	Parallelepiped				Long elliptic cylinder			
	D $[N]$	D_b $[N]$	C_D	C_{D_b}	D $[N]$	D_b $[N]$	C_D	C_{D_b}
1	147.48	53.52	1.768	0.642	126.80	63.17	1.521	0.758
1.2	214.57	63.19	1.787	0.526	182.34	73.18	1.544	0.620
1.5	338.42	75.61	1.804	0.403	288.59	84.29	1.538	0.449
1.8	485.03	83.50	1.795	0.309	408.01	90.34	1.510	0.334
2	593.66	86.12	1.780	0.258	497.38	92.21	1.491	0.276

Tab. 2. Drag and drag coefficient as function of Mach number for long elliptic cylinder and parallelepiped by CFD.

Although all of chosen bodies have the same dimensions, short elliptic cylinder has the lowest base drag coefficient and long elliptic cylinder has the highest base drag coefficient.

Base drag coefficients of short elliptic cylinder and parallelepiped are slightly different and the difference is lower than 5%. It is noticed that bodies with flat base have lower base drag than bodies with rounded rear surface, for bodies with same reference area. Share of base drag to total drag of body depending on Mach number is shown at Fig. 3.

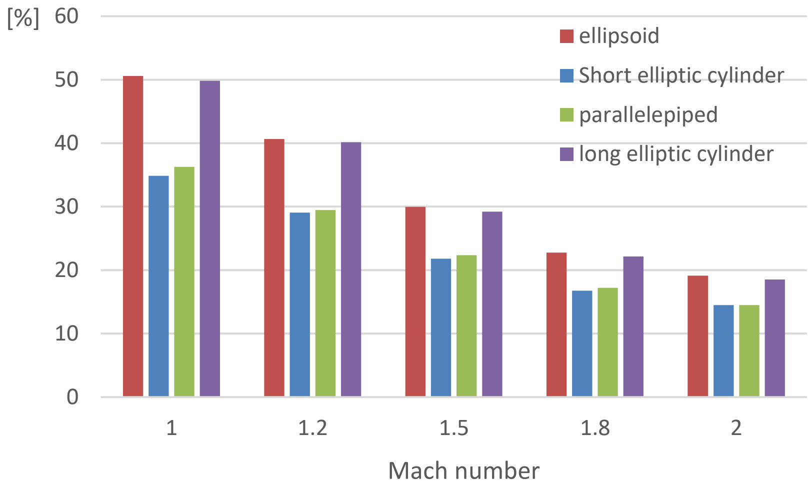

Fig. 3. Share of base drag to total drag of body for $1 \leq M \leq 2$

At $M = 1$, base drag of ellipsoid is 50.6% of total drag, base drag of long elliptic cylinder is 49.8% of total drag, base drag of short elliptic cylinder is 34,9% of total drag and base drag of parallelepiped is 36.3% of total drag. As flow velocity decreases than share of base drag at total drag increases and for $M = 1.5$ it is between 21.8% for short elliptic cylinder and 30% for ellipsoid, and for $M = 2$ it is between 14.5% and 19.1% for chosen bodies.

Flow field around body (Fig. 4 – 7) is shown by vector of velocity coloured by static pressure for the reason that it could be observed recirculation region behind body. Vectors of velocity, coloured by static pressure, around ellipsoid for $M = 1.5$ on length-width plane and on the length-high plane is shown on Fig. 4.

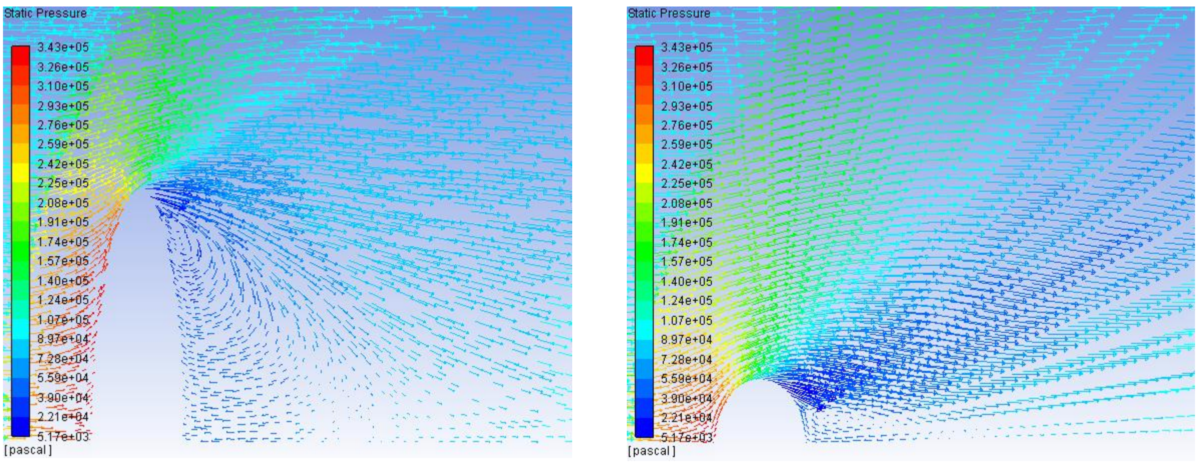

length-width plane length-high plane

Fig. 4. Vectors of velocity, coloured by pressure, around ellipsoid for $M = 1.5$

Flow field as velocity vectors, coloured by static pressure, around short elliptic cylinder is shown on Fig. 5.

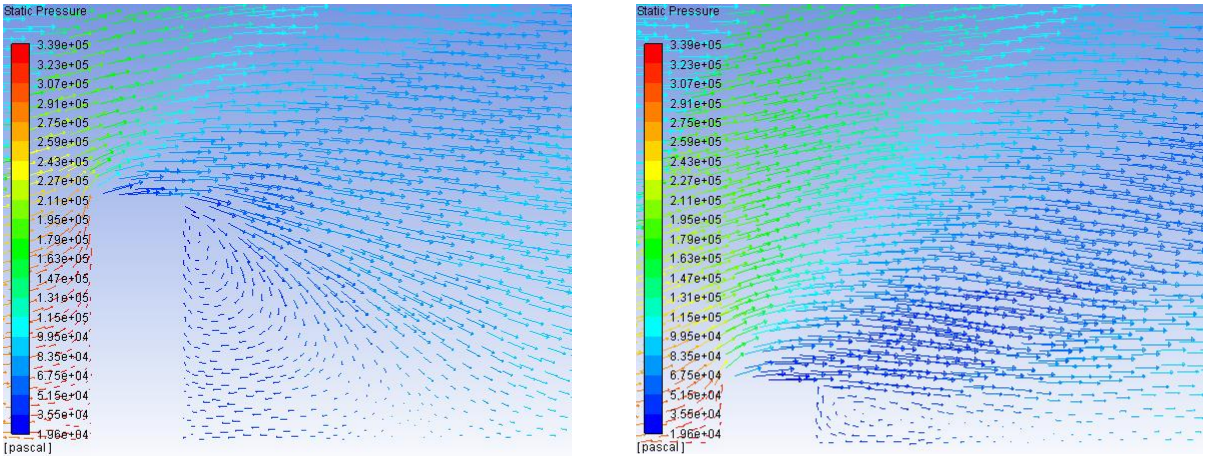

length-width plane length-high plane

Fig. 5. Vectors of velocity, coloured by pressure, around short elliptic cylinder for $M = 1.5$

Ellipsoid and short elliptic cylinder have same reference area, rear surface of ellipsoid is rounded and rear surface of short elliptic cylinder is flat with sharp edge. Pressure on the rear surface of short elliptic cylinder is higher than pressure on the rear surface of ellipsoid resulting lower base drag force and therefore lower base drag coefficient of short elliptic cylinder.

Flow field as velocity vectors, coloured by static pressure, around parallelepiped is shown on Fig. 6.

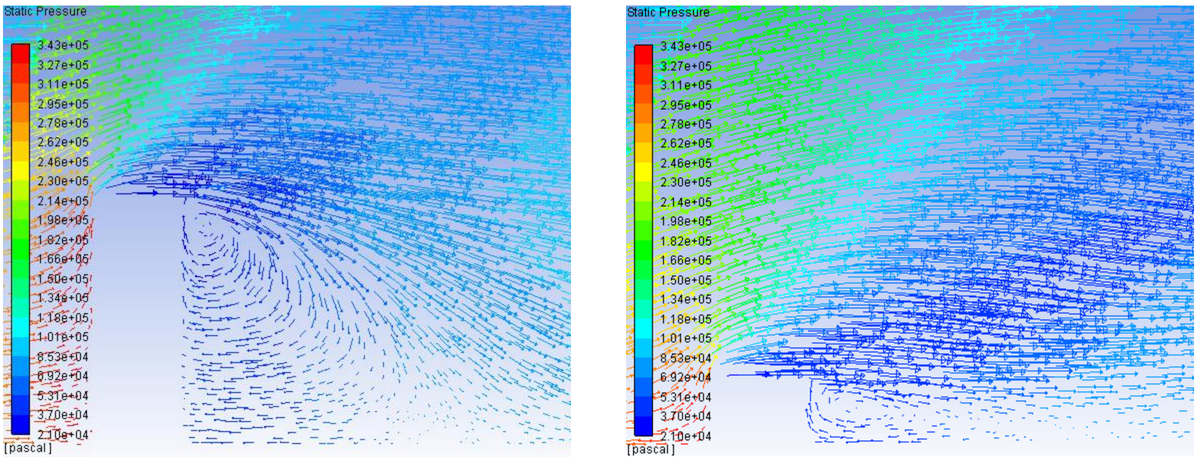

length-width plane length-high plane

Fig. 6. Vectors of velocity, coloured by pressure, around parallelepiped for $M = 1.5$

For parallelepiped and long elliptic cylinder their reference areas are shaped as rectangle with the same dimensions. Parallelepiped has flat rear surface and long elliptic cylinder has rounded rear surface with 2 flat surfaces with sharp edge and 2 continuous transitions from front to rear surface.

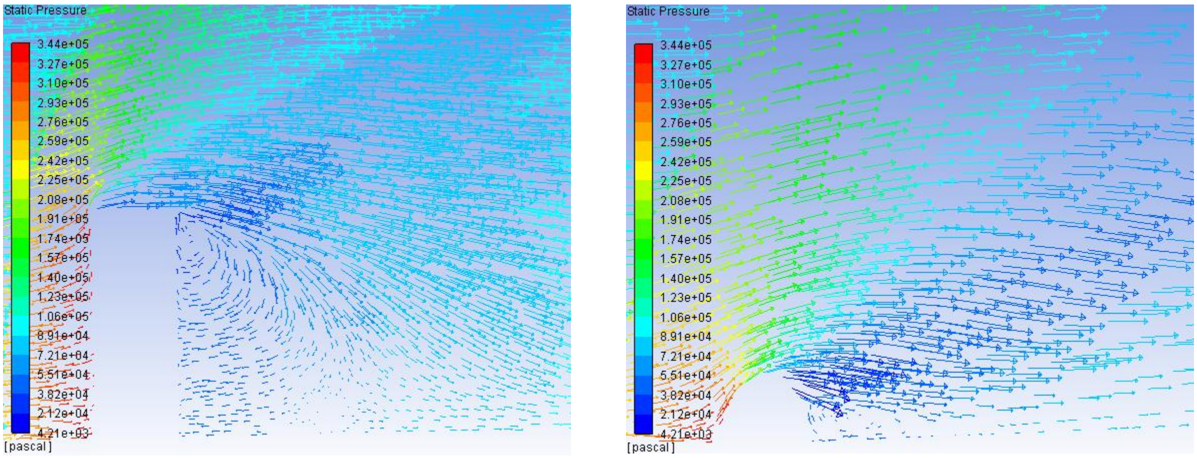

length-width plane length-high plane

Fig. 7. Vectors of velocity, coloured by pressure, around long elliptic cylinder for $M = 1.5$

Pressure at the rear surface of parallelepiped (Fig. 6) is higher than pressure at the rear surface of long elliptic cylinder (Fig. 7), so base drag coefficient of parallelepiped is lower than base drag coefficient of long elliptic cylinder.

4. Conclusion

Four series of numerical computations were made for noncircular irregular shaped bodies at transonic and supersonic speeds, $1 \leq M \leq 2$. Bodies with same width, high and length and different shape (ellipsoid, short elliptic cylinder, long elliptic cylinder and parallelepiped) were chosen. Ellipsoid and short elliptic cylinder have cross section area in the shape of an ellipse and long elliptic cylinder and parallelepiped have cross section area in the shape of rectangle. Rear surface of ellipsoid and long elliptic cylinder is rounded and rear surface of short elliptic cylinder and parallelepiped is flat.

Base drag and base drag coefficient and their share in drag force and drag coefficient were analysed with respect to flow velocity and rear surface curvature of body.

At $M = 1$, base drag of bodies with rounded rear surface is approximately 50% of total drag and base drag of bodies with flat rear surface base drag is about 35% of total drag. As the Mach number increases, the share of the base drag in the total drag decreases.

Short elliptic cylinder has minimum base drag coefficient and long elliptic cylinder has maximum base drag coefficient at transonic and supersonic regimes. It was noticed that rear surface curvature of body at transonic and supersonic speeds has significant influence to base drag coefficient. Aerodynamic base drag coefficient of body is lower in case of flat rear surface than in the case of rounded rear surface.

Future work will be simulation supersonic flow around bodies with same shape, same width and height and higher length to separate effect of length of body to base drag coefficient for body with noncircular cross area.

In addition, it would be good to consider the drag coefficient and its components (wave drag coefficient and base drag coefficient) of chosen bodies for angle of attack of 90° to determine the range of minimum and maximum values.

5. References

Gatski T. B. & Bonnet J.P. (2013). Compressibility, Turbulence and High Speed Flow, ISBN 978-0-12-397027-5, Academic Press, 2nd edition

Jorgensen, L. H. (1973). A Method for Estimating Static Aerodynamic Characteristics for Slender Bodies of Circular and Noncircular Cross Section Alone and with Lifting Surfaces at Angles of Attack from 0° to 90°, NASA TN D-7228

Kljuno, E. & Catovic, A. (2019). A generalized model for estimation of aerodynamic forces and moments for irregularly shaped bodies. Defence Technology, 15(3): 369-389

McCleskey, F. (1988). Drag coefficients for irregular fragments (No. NSWC-TR-87-89). Naval Surface Warfare Center Dahlgren, Naval base in Virginia, Dahlgren, USA.

Moore, F. G. (2000). Approximate Methods for Weapon Aerodynamics. Progress in Astronautics and Aeronautics, American Institute of Aeronautics and Astronautics, Inc.

Moxnes, J. F.; Frøyland, Ø.; Øye, I. J.; Brate, T. I.; Friis, E.; Ødegårdstuen, G. & Risdal, T. H. (2017). Projected area and drag coefficient of high velocity irregular fragments that rotate or tumble. Defence Technology, 13(4): 269-280.

Murman, S. (2010). Lift and drag behavior of unconstrained bluff bodies. The National Aeronautics and Space Administration (NASA/TM-2010-216406), Washington, D.C., USA.

Serdarevic-Kadic, S. & Terzic, J. (2019). Effects of base shape to drag at transonic and supersonic speeds by CFD, Chapter 06 in DAAAM International Scientific Book 2019, pp. 071-081, B. Katalinic (Ed.), Published by DAAAM International, ISBN 978-3-902734-24-2, ISSN 1726-9687, Vienna, Austria

Sivasubramanian, J. & Fasel. H. F. (2006). LES and DES of High Reynolds Number, Supersonic Base Flows with Control of the Near Wake, HPCMP Users Group Conference (HPCMP-UGC'06) 0-7695-2797-3/06 IEEE

Suliman, M. A.; Mahmoud, O. K.; Al-Sanabawy, M.A. & Abdel-Hamid, O. E. (2009). Computational Investigation of Base Drag Reduction for a Projectile at Different Flight Regimes, In: 13th International Conference on Aerospace Sciences & Aviation Technology, Military Technical College, Kobry Elkobbah, Cairo, Egypt

Twisdale, L. A. & Vickery, P. J. (1992). Comparison of debris trajectory models for explosive safety hazard analysis. In the 25th DoD Explosive Safety Conference, Applied Research Associates Inc., Anaheim, California, USA